

Published in final edited form as:

*Biomaterials*. 2009 June ; 30(17): 3058–3067. doi:10.1016/j.biomaterials.2009.01.054.

## Optimization strategies for electrospun silk fibroin tissue engineering scaffolds

Anne J. Meinel<sup>1</sup>, Kristopher E. Kubow<sup>2</sup>, Enrico Klotzsch<sup>2</sup>, Marcos Garcia-Fuentes<sup>1</sup>, Michael L. Smith<sup>2</sup>, Viola Vogel<sup>2</sup>, Hans P. Merkle<sup>1</sup>, and Lorenz Meinel<sup>1,\*</sup>

<sup>1</sup>Institute of Pharmaceutical Sciences, ETH Zurich, Wolfgang-Pauli-Strasse 10, CH-8093 Zurich, Switzerland <sup>2</sup>Laboratory for Biologically Oriented Materials, ETH Zurich, Wolfgang-Pauli-Strasse 10, CH-8093 Zurich, Switzerland

### Abstract

As a contribution to the functionality of scaffolds in tissue engineering, here we report on advanced scaffold design through introduction and evaluation of topographical, mechanical and chemical cues. For scaffolding, we used silk fibroin (SF), a well established biomaterial. Biomimetic alignment of fibers was achieved as a function of the rotational speed of the cylindrical target during electrospinning of a SF solution blended with polyethylene oxide. Seeding fibrous SF scaffolds with human mesenchymal stem cells (hMSC) demonstrated that fiber alignment could guide hMSC morphology and orientation demonstrating the impact of scaffold topography on the engineering of oriented tissues. Beyond currently established methodologies to measure bulk properties, we assessed the mechanical properties of the fibers by conducting extension at breakage experiments on the level of single fibers. Chemical modification of the scaffolds was tested using donor/acceptor fluorophore labeled fibronectin. Fluorescence resonance energy transfer imaging allowed to assess the conformation of fibronectin when adsorbed on the SF scaffolds, and demonstrated an intermediate extension level of its subunits. Biological assays based on hMSC showed enhanced cellular adhesion and spreading as a result of fibronectin adsorbed on the scaffolds. Our studies demonstrate the versatility of SF as a biomaterial to engineer modified fibrous scaffolds and underscore the use of biofunctionally relevant analytical assays to optimize fibrous biomaterial scaffolds.

### Introduction

Appropriate biomaterial scaffolds for tissue engineering purposes should be designed such that they control cellular adhesion, proliferation and differentiation, thereby guiding new tissue formation and function [1]. To meet such specifications, it is necessary to control the chemical, topographical and mechanical properties of the scaffold [2, 3]. This is particularly important for cells with high plasticity such as stem cells, which may give rise to the generation of various tissues depending on the environment which they are exposed to [4–6]. In this context, silk fibroin (SF) has been established as an attractive biomaterial for

© 2008 Elsevier Ltd. All rights reserved.

\*Please direct correspondence to, Priv.Do. Dr. Lorenz Meinel, ETH Zurich, Department for Chemistry and Applied Biosciences, HCI J 390.1, Wolfgang-Pauli-Str. 10, CH-8093 Zurich, Switzerland, tel.: +41 44 633 73 11, fax: +41 44 633 13 14, lorenz.meinel@pharma.ethz.ch.

**Publisher's Disclaimer:** This is a PDF file of an unedited manuscript that has been accepted for publication. As a service to our customers we are providing this early version of the manuscript. The manuscript will undergo copyediting, typesetting, and review of the resulting proof before it is published in its final citable form. Please note that during the production process errors may be discovered which could affect the content, and all legal disclaimers that apply to the journal pertain.

scaffolding [7]. Versatile processing options allow the engineering of tailored architecture, mechanical properties and surface modifications. Furthermore, as a biomaterial, SF features excellent biocompatibility, adaptable biodegradability and good oxygen/water vapor permeability [8–10]. Several studies have detailed its suitability as a template for stem cell based tissue engineering and have suggested its potential towards the controlled generation of bone-, cartilage- or ligament-like tissues [8, 11].

Recent studies demonstrated the impact of topographical cues on cellular performance. For example, nanocolumns affected fibroblast morphology and gene expression, and synthetic nanogratings improved differentiation of human mesenchymal stem cells (hMSC) into neuronal lineages as compared to unpatterned controls [6, 12]. Various techniques to fabricate topographical patterns have been reported, including lithography, polymer demixing, electrospinning, and self-assembly [13]. Electrospinning is a straightforward technique for the fabrication of nanofibrous scaffolds for tissue engineering [14], and can be used to generate 2D and 3D constructs, such as sheets, tubes, stacked sheets and wrapped sheets. Electrospun scaffolds can be manufactured to mimic topographic features of the extracellular matrix (ECM), for example of *in vivo* collagen fibers [15]. Typically, randomly distributed fibers are collected during electrospinning, forming non-woven fibrous mats. However, control of fiber alignment during electrospinning offers the potential to mimic oriented tissue architecture such as found in ligament or muscle tissue [16, 17]. So far the potential of biomimetic fiber alignment on the formation of oriented tissue has been studied with synthetic polymer nanofibers or rapidly degrading biopolymers of low mechanical resilience such as type I collagen [18]. Within this context, studies using more stable biopolymer scaffolds, such as SF, are missing.

Scaffolds for tissue engineering may also be tailored regarding mechanical cues. For example, it is well known that the stiffness of an underlying matrix impacts a number of fundamental biological processes of cells, including differentiation, matrix remodeling and cell migration [4, 19, 20]. The mechanical properties of electrospun fibers are a result of material selection, or can be controlled by modifying the processing parameters and postspinning treatments [21]. Current mechanical assessments of fibrous scaffolds are based on bulk measurements and do not provide information on the single-fiber level. Beyond that, an evaluation of single-fiber mechanics could be a valuable supplement to current bulk assessments, particularly when it comes to probe the microenvironment cells encounter upon adhesion.

Finally, introducing chemical cues into a scaffold requires a substrate that allows physical adsorption or covalent decoration with short recognition sequences or ECM molecules to the surface, as previously shown for SF [22, 23]. For instance, to mediate outside-in and inside-out signaling, short Arg-Gly-Asp (RGD) motifs as well as whole ECM molecules such as fibronectin may serve as cellular binding sites for integrin receptors and impact cellular adhesion, migration, growth and differentiation [24]. Despite a limited number of studies describing the use of SF fibers coated with ECM proteins for the support of cellular interactions [25, 26], more detailed studies about the conformation and biological impact of adsorbed proteins on SF fibers are critical to improve control and guidance of the cell response to such scaffolds. For instance, fibronectin is a multidomain ECM protein with several molecular recognition sites functioning as chemical cues. Conformational changes to fibronectin upon adsorption to model surfaces with different chemical composition were shown to cause exposure of cryptic binding sites which led to different integrin binding specificity affecting myoblast differentiation [27]. Therefore, precise control of the conformational state of such ECM proteins, when decorating biomaterials, may be essential to control the biological performance of such implants and their *in vivo* success [28].

In this study, we introduce and evaluate multiple means to engineer environmental cues into SF scaffolds. A rotating target is used to control scaffold topography by SF fiber alignment during electrospinning. Postspinning treatments are applied to SF fibers, and their mechanical properties are tested as extension at breakage of single fibers. To improve cellular spreading on SF fibers we decorate them with fibronectin as a chemical cue, and study its conformational state upon adsorption. The cellular response to such scaffolds is analyzed *in vitro* using hMSC cultures, an important human progenitor cell source for tissue engineering.

## Materials and Methods

### Materials

*Bombyx mori* (silk worm) cocoons were from Trudel Inc Zurich, Switzerland. Surface antigen antibodies for flow cytometry were obtained from Becton Dickinson (Allschwil, Switzerland) and papain was from Worthington Biochemical Corporation (Allschwil, Switzerland). Fetal bovine serum (FBS), Dulbecco's modified eagle medium (DMEM), Roswell Park Memorial Institute medium (RPMI-1640), basic fibroblast growth factor (bFGF), penicillin, D-streptomycin, fungizone, nonessential amino acids (NEAA, consisting of 8.9 mg/L L-alanine, 13.21 mg/L L-asparagine, 13.3 mg/L L-aspartic acid, 14.7 mg/L L-glutamic acid, 7.5 mg/L glycine, 11.5 mg/L L-proline, 10.5 mg/L L-serine) and trypsin were purchased from Gibco (Carlsbad, CA). Transforming growth factor-1 (TGF-1) was obtained from R&D Systems (Abingdon, UK) and BMP-2 was kindly supplied by Wyeth (Andover, MA). 3-[2-(2-aminoethylamino)ethyl-amino]propyl-trimethoxysilane was from AcrosOrganics (Geel, Belgium). All other substances were of analytical or pharmaceutical grade and obtained from Sigma (St. Louis, MO).

**Preparation of regenerated *Bombyx mori* silk fibroin solution**—SF was prepared using a modification of our earlier procedure [29]. Briefly, cocoons from *Bombyx mori* were boiled in an aqueous solution of 0.02 M Na<sub>2</sub>CO<sub>3</sub>, rinsed with ultrapurified water (UPW) and dissolved in 9 M LiBr at 55°C to generate a 10% w/v solution. This solution was dialyzed (Pierce, Rockford, IL, MWCO 3.500 Da) against UPW for 48 h. After desalination a second dialysis step against PEG 6,000 (200 g/1.5 l UPW) was performed to generate a SF solution of higher concentration which was determined by weighing the remaining solid after drying. SF solution of 12.5% w/w was obtained by diluting the concentrated SF solution with UPW.

A SF/PEO blend was used for electrospinning to enable stable, continuous spinning [30]. PEO 900,000 solution of 5% w/w was prepared by directly adding PEO to UPW and stirring for 5 days at room temperature. The solution was filtered through a 5 µm syringe filter to remove remaining insoluble materials. 2 ml of PEO solution (5% w/w) were mixed with 5 ml of SF solution (12.5%) by moderate stirring for further use in the electrospinning process.

**Electrospinning**—Electrospinning was performed in a fume hood using a cylindrical target to collect fibers except for mechanical measurements using a similar setup as described before [25]. Relative humidity was adjusted by flushing the hood with dry air. A volume flow rate of 1.2 ml/h of the SF/PEO blend through a steel capillary tube was maintained using a syringe pump. For electrospinning a voltage of 12–15 kV was applied to the capillary tube using a high voltage power supply (Fabrimex, Volketswil, Switzerland). The distance between the capillary tube and the grounded target was 19 cm. Randomly oriented fibrous scaffolds were collected on a cylindrical target of  $d = 3.8$  cm when rotating at 200–250 min<sup>-1</sup>, whereas aligned fibrous scaffolds were collected on a cylindrical target of  $d = 14$  cm rotating at 1000 up to 4000 min<sup>-1</sup>.

**Fiber treatment and fiber characterization**—Electrospun fibrous scaffolds from the SF/PEO blend were either immersed in 90/10 (v/v) methanol/water for 30 min (MeOH treatment) or stored for 12 h in a desiccator containing a saturated aqueous solution of  $\text{Na}_2\text{SO}_4 \times 10 \text{ H}_2\text{O}$  at room temperature (93% relative humidity, water vapor treatment) to induce an amorphous to beta-sheet transition of SF [31]. Fibrous scaffolds were washed with UPW for 48 h at 37°C to remove PEO [32].

Scanning electron microscopy (SEM) was used to determine the diameter of electrospun fibers and surface texture of fibers was examined after treatments with methanol or water vapor and washing for 48 h. Samples were coated with platinum prior to evaluation with a LEO 1530 GEMINI scanning electron microscope (Zeiss, Cambridge, UK).

Fourier transformed infrared spectroscopy (FT-IR) data were gathered on a Nicolet 5.700-spectrometer (Thermo Fisher Scientific, Waltham, MA). Samples were compressed into KBr pellets and each spectrum was acquired in transmittance mode by accumulation of 256 scans with a resolution of  $2 \text{ cm}^{-1}$  and a spectral range of 4,000 to  $400 \text{ cm}^{-1}$ .

**Mechanical measurements on single fibers**—Thin polydimethylsiloxane (PDMS) grids with 40  $\mu\text{m}$  wide and 12  $\mu\text{m}$  deep trenches were prepared similar to a method previously described [33]. For covalent attachment of SF fibers onto the grids, plasma-cleaned grids were functionalized with 3-[2-(2-aminoethylamino)ethyl-amino]propyl-trimethoxysilane (3% in UPW; 15 min) and activated with glutaraldehyde (0.5% in UPW, 30 min). Finally, the grids were rinsed with UPW and dried. Fibers were electrospun from a SF/PEO blend with a flow rate of 0.8 ml/h onto the PDMS grids which were fixed between two parallel grounded metal clamps to deposit a few isolated fibers perpendicular to the grid structure. Postspinning treatments of fibers on PDMS grids were performed as described above using either MeOH or water vapor and subsequent washing with UPW.

A 3-axis micromanipulator (Sutter Instrument, Novato, CA) with a thin tungsten probe attached (Nanoprobes, NY) was used to stretch single SF fibers [34]. A schematic image of the setup is shown as insert in Figure 3. Tip displacement along the trenches was programmed to proceed at 2  $\mu\text{m}/\text{step}$ . DIC movies were recorded with an Olympus FV 1000 confocal microscope (Olympus, Volketswil, Switzerland) to analyze maximum fiber extension at breakage, and samples were kept in UPW throughout. 4 batches of fibers were prepared and only fibers which showed no detachment from PDMS grids before breakage were included in the analysis ( $n=10-17$  per batch).

**Fibronectin adsorption onto electrospun SF scaffolds and evaluation by fluorescence resonance energy transfer (FRET) imaging**—Human plasma fibronectin was isolated from fresh human plasma [35] and double labeled with acceptor fluorophores (Alexa 546, Molecular Probes, Eugene, OR) on free cysteines, and with donor fluorophores on random amines (Alexa 488, Molecular Probes, Eugene, OR), as previously described [35–37]. Labeling yielded an average of 6.3 donor and 3.6 acceptor moieties per fibronectin molecule. Acquisition of FRET images was by means of confocal laser scanning microscopy (CLSM). Acceptor and donor intensities were separately detected using 10 nm donor (515–525 nm) and acceptor (567–577 nm) emission peaks. Since individual fibronectin molecules within the multi-labeled fibronectin population carried different fluorophore labeling ratios, absolute distances between donor and acceptor fluorophores could not be calculated. Instead the ratio of acceptor to donor fluorophore intensities ( $I_A/I_D$ ) was measured as an indication of average fluorophore separation and hence fibronectin conformation.

The sensitivity of double labeled fibronectin (fibronectin-D/A) to unfolding was evaluated by progressively denaturing fibronectin-D/A in a series of GdnHCl concentrations from 0 to 4 M [35]. For  $I_A/I_D$  measurements of fibronectin-D/A on SF scaffolds, scaffolds were immersed in fibronectin solution (20  $\mu\text{g}/\text{ml}$  in phosphate buffer solution, PBS) for 75 min and labeled fibronectin was diluted with unlabeled fibronectin (10:90) to avoid intermolecular FRET [35]. Scaffolds were washed with PBS and placed in a MatTek glass bottom culture dish (MatTek, Ashland, MA) filled with PBS for imaging.

All images were processed with Matlab software (Mathworks, Bern, Switzerland). Dark current background values were subtracted from donor and acceptor images and a threshold mask of 100 relative intensity units was applied to all images of Fn-D/A on SF scaffolds [35]. Then, acceptor images were divided pixel by pixel by donor images and histograms were computed from all data pixels within each field of view.

#### **Primary human mesenchymal stem cell (hMSC) isolation and expansion—**

Total human bone marrow (25  $\text{cm}^3$ , Cambrex, Walkersville, MD) was diluted in isolation medium (5% FBS in RPMI-1640 medium) and centrifuged at  $300 \times g$  for 10 min. Cells were pelleted and resuspended in expansion medium (DMEM, 10% FBS, 100 U/ml penicillin, 1000 U/ml streptomycin, 0.5  $\mu\text{g}/\text{ml}$  fungizone antimycotic, 1% NEAA, 1 ng/ml bFGF) and seeded in 175  $\text{cm}^2$  flasks at a density of  $5 \times 10^4$  cells/ $\text{cm}^2$ . Adherent cells were allowed to reach 80% confluence (15 days for passage 0). Cells were trypsinized and replated every 7–8 days. Second or third passage (P2, P3) cells were used for cell culture experiments. The expression of the surface antigens CD31, CD34 and CD105 was characterized by flow cytometry (FacsCanto, Becton Dickinson, Basel, Switzerland), similar to what was previously described [11]. Briefly, trypsinized cells were pelleted and resuspended in RPMI medium with 10% FBS at a concentration of  $1 \times 10^7$  cells/ml. Aliquots of the cell suspension were incubated with R-Pe conjugated anti-CD31 (PECAM-1/endothelial cells), APC conjugated anti-CD34 (sialomucin/hematopoietic progenitor cells) and anti-CD105 (endoglin/endothelial cells and hMSC) with a secondary goat-antimouse IgG FITC-conjugated antibody. Cells were washed and fixed with 2 % formalin before analysis.

To assess the potential of hMSC for osteogenic and chondrogenic differentiation, the cells were cultured in 12-well plates as micro-mass cultures (2 drops of 15  $\mu\text{l}$  of  $2 \times 10^7$  cells/ml per well) in either control medium (DMEM, 10% FBS, 100 U/ml penicillin, 1000 U/ml streptomycin, 0.5  $\mu\text{g}/\text{ml}$  fungizone antimycotic), osteogenic medium (control medium supplemented with 50  $\mu\text{g}/\text{ml}$  ascorbic acid-2-phosphate, 10 nM dexamethasone, 10 mM  $\beta$ -glycerolphosphate, and 1  $\mu\text{g}/\text{ml}$  BMP-2) or chondrogenic medium (control medium supplemented with 50  $\mu\text{g}/\text{ml}$  ascorbic acid-2-phosphate, 10 nM dexamethasone, 1% NEAA, 5  $\mu\text{g}/\text{ml}$  insulin, and 5 ng/ml TGF- $\beta_1$ ). Medium was exchanged 3 times per week. After 3 weeks of culture the pellets were washed in PBS and the amounts of glycosaminoglycans (GAG) and calcium were measured. For the determination of calcium content micro-mass cultures were extracted with 0.5 ml 5% trichloroacetic acid and calcium was measured spectrophotometrically at 570 nm (Thermomax microplate reader, Molecular Devices, Sunnyvale, CA) following the reaction with o-cresolphthalein complexone according to the manufacturer's protocol (Rolf Greiner Biochemica, Flacht, Germany). To measure the amount of GAG, samples were digested for 16 h with 0.5 ml papain solution (2.4 U/ml) in buffer (0.1 M disodium hydrogen phosphate, 0.01 M EDTA disodium salt, 14.4 mM L-cysteine) at 60 °C. GAG content was determined spectrophotometrically (Cary 300, Varian, Palo Alto, CA) at 525 nm following binding to the dimethylene blue dye using chondroitin sulphate as standard [38].

**Cell culture on electrospun SF scaffolds—**Disc shaped scaffolds were punched (15 mm in diameter), water vapor treated and used for cell culture after steam autoclaving. For

fibronectin coating, scaffolds were immersed in 20  $\mu\text{g/ml}$  fibronectin in PBS (0.5 ml) for 75 min at RT and rinsed with PBS. hMSC were seeded at a density of  $1 \times 10^5$  cells/scaffold and cultured in control medium at 37°C, 5%  $\text{CO}_2$  on fibronectin-coated or uncoated scaffolds.

**Cell adhesion assay**—Prior to biochemical analysis of adherent cells measured as DNA content on scaffolds, loosely adherent or unbound cells were removed by washing twice with PBS. Scaffolds were transferred into a 0.1% Triton X-100 solution and disintegrated by using steel balls and a Minibead-beater (Biospec, Bartlesville, OK). DNA content was measured using the PicoGreen assay (Molecular Probes, Eugene, OR) according to the manufacturer's protocol. Aliquots of the solutions prepared from the samples ( $n = 4$  per group and timepoint) were measured fluorometrically at an excitation wavelength of 480 nm and an emission wavelength of 520 nm (FluoroCount, Packard BioScience, Meriden, CT).

**Cell spreading analysis**—To determine cell morphology on electrospun SF scaffolds by SEM, samples were rinsed in 0.1 M sodium cacodylate buffer and fixed in glutaraldehyde (1.5% glutaraldehyde in 0.1 M sodium cacodylate solution) at RT for 2 h. Samples were rinsed in 0.1 M sodium cacodylate, dehydrated through exposure to a gradient of alcohol and HMDS and dried in a fume hood before sputter coating with platinum for SEM.

Fluorescent images were acquired after labeling cell membranes with DiI (1,1-dicocadecyl-3,3,3,3-tetramethyl-indocarbocyanine perchlorate, Molecular Probes, Eugene, OR). For this purpose hMSC ( $5 \times 10^5$  cells/ml) were resuspended in 4  $\mu\text{g/ml}$  DiI in control medium, and the cell suspension was incubated for 30 min on a gently rotating shaker at 37°C. Cells were washed 5 times in culture medium and seeded on fibronectin-coated or uncoated scaffolds. Cells were then cultured for 2 h at 37°C, 5%  $\text{CO}_2$ , rinsed with PBS and fixed with 2% formalin for 20 min before imaging.

**Statistical analysis**—Presentation of data is as means  $\pm$  standard deviation (Figure 7). For statistical significance, samples were evaluated using the log rank test based on the Kaplan Meier plot (Figure 3) and the Student t-test (Figure 7). Differences between groups were considered significant for  $p < 0.05$ .

## Results

### Characterization of fibrous scaffolds

Non-woven fibrous scaffolds were prepared by electrospinning of aqueous SF/PEO blends. When using a slowly rotating cylindrical target we obtained porous scaffolds with randomly oriented nanoscale fibers and interconnected voids between fibers. Depending on the relative humidity, uneven and beaded fibers were obtained at 60% RH, while electrospinning below 30% RH resulted in uniform and bead-free fibers that were  $530 \pm 100$  nm in diameter (Figure 1A, B). Therefore, fibers prepared at  $< 30\%$  RH were used for further experiments. The control of fiber network orientation was achieved as a function of the rotational speed of the target (1000 up to 4000  $\text{min}^{-1}$ ). Optimum fiber alignment was achieved at 4000  $\text{min}^{-1}$  as qualitatively assessed (Figure 1C–E).

To investigate conformational changes of SF in fibrous scaffolds after MeOH or water vapor treatment, FT-IR structural analysis was performed (Figure 2A–C). MeOH treatment of electrospun SF scaffolds resulted in a N-H bending vibration bond (amide II) intensity shift from 1539 to 1520  $\text{cm}^{-1}$  compared to untreated scaffolds. For water vapor treated SF scaffolds a peak shift with a maximum at 1531  $\text{cm}^{-1}$  for the amide II band and two shoulders at 1537 and 1520  $\text{cm}^{-1}$  was observed. Similarly, the amide I peak was shifted from 1651 to 1632  $\text{cm}^{-1}$  after treatments with MeOH or water vapor, with the shift being more pronounced for the MeOH treated SF scaffolds. Washing of MeOH or water vapor

treated scaffolds at 37°C for 2 d resulted in the essential absence of typical PEO peaks at 1101 (C-O-C stretching), 953 cm<sup>-1</sup> (CH<sub>2</sub> rocking) and 843 cm<sup>-1</sup> (CH<sub>2</sub> rocking), suggesting that the water soluble PEO had been extracted. Surface texture of electrospun scaffolds was assessed by SEM (Figure 2D–F). A smooth fiber surface was observed after treatment with water vapor whereas MeOH treatment resulted in an increase of surface roughness compared to non treated fibers.

### Extension at breakage of single fibers

Extension at breakage in water was measured for single electrospun fibers after MeOH or water vapor treatment and PEO extraction. This protocol has been previously shown to be applicable for manually deposited fibers of fibronectin [39]. Median extension at breakage was 77–229% for MeOH treated and 152–364% for water vapor treated fibers depending on the variability between batches of measured fibers and without a consistent statistical difference between the two treatments (Figure 3).

### Fibronectin adsorption onto fibrous scaffolds

In order to visualize the spatial distribution of fluorescently labeled fibronectin on SF scaffolds we performed CLSM. We observed uniform coatings of the SF fibers with labeled fibronectin-D/A, as reflected by the net-like fluorescence of the scaffolds (Figure 4A). Scaffolds coated with unlabeled fibronectin did not show any fluorescent signal under the same conditions (negative control, data not shown). To measure the structural changes of fibronectin upon adsorption to the SF surface, we analyzed FRET between multiple donor and acceptor fluorophores attached to fibronectin. Figure 4B and C shows a color-coded ratiometric image of  $I_A/I_D$  values of fluorescently labeled fibronectin-D/A adsorbed on SF, in combination with a histogram indicating a relatively broad distribution for all data pixels. Intensity ratios ( $I_A/I_D$ ) were correlated to known conformations of the protein in increasing concentrations of GdnHCl (Figure 4C) [35, 37]. Median  $I_A/I_D$  values of fibronectin adsorbed on SF scaffolds corresponded to  $I_A/I_D$  scale values between 0 to 1 M GdnHCl. This indicated a partial separation of its dimeric arms, which are crossed over in solution [35].

### hMSC characterization

hMSC were characterized with respect to their expression of surface antigens and the ability to selectively differentiate along the chondrogenic and osteogenic lineages in response to environmental stimuli. GAG accumulation was significantly higher in chondrogenic medium as compared to control medium or osteogenic medium (Figure 5A). Calcium deposition was observed only with hMSC cultured in osteogenic medium, but not in control or chondrogenic medium (Figure 5B). Flow cytometry showed that more than 95% of the cells expressed the surface antigen CD105, a descriptive yet not causal marker for hMSC (Figure 5C). Negative expression of surface antigens CD34 and CD31 suggested the absence of hematopoietic progenitor cells and cells of endothelial origin (Figure 5D, E) [40, 41].

### hMSC response to modified fibrous scaffolds

Modulation of cell-matrix interaction upon fibronectin coating and fiber alignment, was investigated using hMSC on SF scaffolds. Two hours after seeding, cells were well spread on fibronectin-coated random scaffolds and had a flattened shape with cellular extensions (Figure 6). In contrast, cells on scaffolds without fibronectin coating had a spherical morphology. After 72 hours differences in cell shape were indistinguishable among groups with a well spread morphology on all scaffolds.

Measurements of the total DNA content indicated that significantly more cells adhered to fibronectin-coated scaffolds as compared to non-coated scaffolds at the timepoints of 0.5 and 2 h ( $p < 0.01$ ) and 48 h after seeding ( $p < 0.05$ , Figure 7). No significant differences were observed after 1, 8, 24 and 72 h.

The response of hMSC to fiber alignment was studied after 2 h on fibronectin-coated scaffolds. Both SEM and CLSM demonstrated an elongated and spindle-shaped morphology of hMSC on aligned SF fibers with their orientation being parallel to that of the fibers (Figure 8).

## Discussion

Solution parameters (e.g. viscosity, conductivity, surface tension), processing parameters (e.g. electric field strength, flow rate and collector-set up), as well as ambient parameters (e.g. temperature and humidity) impact the process of electrospinning [42–48]. In the present study, air humidity was critical for electrospinning SF fibers. Low humidity was a prerequisite to achieve bead-free fibers (Figure 1A, B). This may be explained by an increased rate of solvent (water) evaporation at dry conditions. At high humidity, solvent removal may have been insufficient between when the jet fluid stream left the spinneret and when it reached the target. This incomplete removal possibly resulted in bead formation due to residual solvent and the resulting high surface tension as has been suggested for the electrospinning of hyaluronic acid [49].

Fiber alignment in scaffolds is considered as a beneficial topographical cue for the engineering of structurally oriented tissue architecture, and may serve as a biomimetic tool to induce phenotypic differentiation of the cells and ensure overall tissue function [16, 50]. Depending on the rotational speed of the cylindrical target the alignment of electrospun SF fibers could be well controlled (Figure 1C–E) as recently also shown for synthetic polymers [51–53]. Limitations in fiber alignment by high rotational speeds, as previously reported for collagen, potentially related to the low fiber strength and elasticity of collagen, were not observed for SF [18]. The results thus demonstrate the superior processability of SF as compared to collagen, and add another biomaterial option to the currently available set of suitable synthetic polymers.

Treatment of SF scaffolds with methanol is frequently used to crystallize SF rendering it insoluble in aqueous media [44]. It is well established that MeOH treatment triggers the transition of SF from a predominantly random coil or silk I structure into a water insoluble  $\beta$ -sheet enriched structure [32, 44]. This also holds true for our electrospun fibrous SF scaffolds as shown by the shifts of the amide I and II bands in their FT-IR spectra (Figure 2A) [30, 32]. Water vapor treatment of the scaffolds resulted in similar shifts of the amide bands (Figure 2B) and presents a milder alternative as compared to treatments with organic solvents, e.g. when labile growth factors are embedded into fibers.

Bulk mechanical properties of electrospun SF scaffolds showed 4.4% and 8.5% extension at breakage for MeOH and water vapor treated scaffolds [54]. Starting off from these observations we scaled the mechanical assessment down to the single fiber level. In these experiments, median extensions at breakage were much higher (77–229% for MeOH treated and 152–364% for water vapor treated fibers). In contrast to the reported bulk assessments, which were performed in dry state at 50% RH [54], single fiber measurements were conducted in water. Similarly high extensions as reported here were previously observed for SF films in water and hydrated electrospun SF tubes after water annealing and MeOH treatment, respectively [55, 56]. A likely explanation for high extensions at breakage in an aqueous environment is the plasticizing effect of water as indicated for fibers from

regenerated spider silk [57]. When compared to bulk measurements in literature [56], our single fiber measurements further suggest that extension at breakage in an aqueous environment is mainly governed by single fiber behavior (or below) and less influenced by fiber orientation, fiber overlay or branch points in the fibrous scaffold. Nevertheless, as concluded from the observed large variabilities of the extension at breakage data, our experimental setup may require further optimization and validation, and different methods for single fiber and bulk measurements have to be taken into account when comparing fibrous material properties. Further use of this method at the interface of single fiber mechanics and cellular performances may extend our understanding how to modulate electrospun biomaterials towards optimized cellular interaction. Within the context of SF, future experiments building off from these findings will correlate the impact of elastic components (such as elastin) or crosslinking of fibers with cell cytoskeleton assembly and differentiation [4, 58].

Decoration of scaffolds with ECM ligands as chemical cues, such as fibronectin, is a biomimetic approach to affect scaffold functionality, e.g., towards an increase in cellular adhesion. The RGD sequence is a well known binding site on fibronectin and other matrix proteins for cell-surface presented integrin receptors [59], but is not present in *Bombyx mori* SF [60]. Therefore, adsorption of fibronectin may offer the potential to increase cellular adhesion to SF scaffolds. However, fibronectin also displays a number of other molecular recognitions sites for cells, e.g., the synergy site (PHSRN), which enhances  $\alpha_5 \beta_1$  integrin binding to the RGD site, and for other ECM components. It is noteworthy that some of these sites are cryptic and that each of them must be in a certain conformation in order to function [61]. Thus, adsorption of fibronectin to a substrate may not only render the surface amenable to cell adhesion, but also changes the conformation of the molecule, which could in turn alters its epitope exposure, leading to altered cell behavior [27, 37, 62]. To investigate the adsorption of fibronectin to the silk scaffolds and the resulting conformational change we used FRET imaging of double fluorophore fibronectin-D/A molecules and studied fibronectin adsorption and related structural changes of the protein. The median intensity ratios of fibronectin-D/A on SF scaffolds (Figure 4B, C) were intermediate between those previously reported for adsorption onto (hydrophilic) glass and (hydrophobic) fluorosilane surfaces [37]. Previous studies showed that cellular adhesion and proliferation increased on more hydrophilic fibronectin-coated surfaces. This was explained by an extension of fibronectin subunits that promotes exposure of previously cryptic cell integrin binding sites [61]. Other experiments have shown that surface chemistry, charge and topography of a substrate may affect the ability of fibronectin to mediate cell spreading, proliferation and differentiation. In fact, C2C12 myoblasts were reported to proliferate or differentiate on fibronectin-coated model surfaces as a function of fibronectin conformation [27, 63, 64]. Further studies are needed to correlate fibronectin conformation on different scaffold materials with cell response to these substrates *in vitro* and *in vivo* in order to use FRET as a routine probe to predict a scaffold's biological performance.

Cell culture experiments were performed with hMSC isolated from adult human bone marrow. This cell source is well established for tissue engineering applications, based on its marked proliferation and differentiation potential (Figure 5) [65]. hMSC also express numerous integrins on their cell surface and secret various ECM components [66, 67]. In this study on fibronectin-coated fibrous SF scaffolds, hMSC showed a clear response to the fibronectin coating, undergoing rapid adhesion and advanced spreading within 2 h of culture as compared to non fibronectin-coated scaffolds (Figures 5,6). This contrasts with a previous study, in which only minor differences in terms of adhesion and spreading were observed for normal human epidermal keratinocytes or fibroblasts after 1 h of cell culture on fibronectin-coated or non-coated SF fibers [25]. A possible explanation for the discrepancy may be that keratinocytes and fibroblasts expressed a different mosaic of integrin receptors on their

surfaces as compared to hMSC. Furthermore, in the previous study the aforementioned surface-dependent fibronectin conformation and especially the low coating density may not have supported cellular adhesion to the same extent as observed here [25].

After an extended culture period of 72 h, differences in hMSC adhesion between fibronectin-coated and non-coated scaffolds leveled off. Cell spreading was similar for hMSC cultured on fibronectin-coated or non-coated scaffolds (Figures 6,7). This finding could have been the result of cellular secretion of ECM molecules from hMSC over time and/or serum protein adsorption from the culture medium, both of which would quickly outweigh the initial advantage of a fibronectin-coated surface. A similar effect has been observed on RGD-functionalized surfaces, which facilitated enhanced fibroblast adhesion relative to unmodified surfaces up to 2 h in serum containing medium, but exhibited no significant difference thereafter [68].

hMSC morphology on electrospun scaffolds largely depended on scaffold architecture, namely whether it consisted of randomly oriented or aligned SF fibers. The latter typically resulted in elongated cell morphology and orientation along the main fiber axis (Figure 8). This corroborates previous studies made with other cells, such as coronary artery endothelial cells, cardiomyocytes and ligament fibroblasts [16, 69–71]. The preferred cell orientation on aligned fibers was also observed after hMSC differentiation (in preliminary experiments in mixed adipogenic/osteogenic differentiation medium, data not shown). Given the expansion and multilineage potential of hMSC to generate tissues of different type and structure, scaffolds with topographical guidance may prove useful in the engineering of structured tissues, e.g. ligament or muscle. Changes beyond cellular morphology were demonstrated for other cell types, such as fibroblasts and MC3T3-E1 cells aligned on nanofibers or microgrooves impacting cellular metabolism and resulting in an increased and oriented deposition of a collagen matrix [16, 72]. Similar effects have yet to be studied for hMSC on aligned fibers.

## Conclusions

This study explored optimization strategies for scaffold design by introduction and evaluation of topographical, mechanical and chemical cues. We used advanced analytical tools shifting mechanical evaluation from bulk properties down to the single fiber level. The topography of electrospun scaffolds was impacted by electrospinning conditions, particularly the rotational speed of the cylindrical target. SF fiber alignment functioned as topographical cue leading to elongated and oriented cellular morphologies and may open an interesting avenue to use SF scaffolds for the *de novo* engineering of structurally aligned tissues. Fibronectin adsorbed on SF scaffolds was demonstrated by FRET to exhibit partial extension of its dimer arms and functioned as a chemical cue to enhance hMSC adhesion and spreading. Relating biologically relevant protein conformations on scaffolds to cell responses can provide a useful tool to further optimize scaffold surfaces towards enhanced biological features. In conclusion, our findings pave the way for more generally applicable optimization strategies for biomaterial scaffold design. We thus suggest to further explore the potential of these scaffolds for tissue engineering applications *in vitro* and *in vivo*.

## Acknowledgments

We thank Marc Simonet for helpful advice with the electrospinning and Sheila Luna for providing the schematic images in Figures 3 and 4. We further thank Trudel Inc. (Zurich, Switzerland) for the supply of silk cocoons and Wyeth pharmaceuticals (Andover, MA) for providing BMP-2. Funding by the BEST Bioengineering Cluster for AJM and by the Human Frontier Science Program Organization for MLS is greatly acknowledged.

## References

1. Muschler GF, Nakamoto C, Griffith LG. Engineering principles of clinical cell-based tissue engineering. *J Bone Joint Surg Am.* 2004 Jul; 86-A(7):1541–1558. [PubMed: 15252108]
2. Toh Y, Ng S, Khong YM, Zhang X, Zhu Y, Lin P, et al. Cellular response to a nanofibrous environment. *Nanotoday.* 2006; 1(3):34–43.
3. Wong YW, Leach JB, Brown XQ. Balance of chemistry, topography, and mechanics at the cell-biomaterial interface: Issues and challenges for assessing the role of substrate mechanics on cell response. *Surface Science.* 2004; (570):119–133.
4. Engler AJ, Sen S, Sweeney HL, Discher DE. Matrix elasticity directs stem cell lineage specification. *Cell.* 2006 Aug 25; 126(4):677–689. [PubMed: 16923388]
5. Salaszyk RM, Williams WA, Boskey A, Batorsky A, Plopper GE. Adhesion to Vitronectin and Collagen I Promotes Osteogenic Differentiation of Human Mesenchymal Stem Cells. *J Biomed Biotechnol.* 2004; 2004(1):24–34. [PubMed: 15123885]
6. Yim EKF, Pang SW, Leong KW. Synthetic nanostructures inducing differentiation of human mesenchymal stem cells into neuronal lineage. *Exp Cell Res.* 2007; 313(9):1820–1829. [PubMed: 17428465]
7. Altman GH, Diaz F, Jakuba C, Calabro T, Horan RL, Chen J, et al. Silk-based biomaterials. *Biomaterials.* 2003 Feb; 24(3):401–416. [PubMed: 12423595]
8. Meinel L, Hofmann S, Karageorgiou V, Kirker-Head C, McCool J, Gronowicz G, et al. The inflammatory responses to silk films in vitro and in vivo. *Biomaterials.* 2005 Jan; 26(2):147–155. [PubMed: 15207461]
9. Wang Y, Kim HJ, Vunjak-Novakovic G, Kaplan DL. Stem cell-based tissue engineering with silk biomaterials. *Biomaterials.* 2006 Aug 4.
10. Minoura N, Tsukada M, Nagura M. Physico-chemical properties of silk fibroin membrane as a biomaterial. *Biomaterials.* 1990; 11(6):430–434. [PubMed: 2207234]
11. Meinel L, Karageorgiou V, Hofmann S, Fajardo R, Snyder B, Li C, et al. Engineering bone-like tissue in vitro using human bone marrow stem cells and silk scaffolds. *J Biomed Mater Res A.* 2004 Oct 1; 71(1):25–34. [PubMed: 15316936]
12. Dalby MJ, Riehle MO, Sutherland DS, Agheli H, Curtis AS. Morphological and microarray analysis of human fibroblasts cultured on nanocolumns produced by colloidal lithography. *Eur Cell Mater.* 2005; 9:1–8. discussion 8. [PubMed: 15690263]
13. Stevens MM, George JH. Exploring and engineering the cell surface interface. *Science.* 2005 Nov 18; 310(5751):1135–1138. [PubMed: 16293749]
14. Ma Z, Kotaki M, Inai R, Ramakrishna S. Potential of nanofiber matrix as tissue-engineering scaffolds. *Tissue Eng.* 2005 Jan-Feb; 11(1–2):101–109. [PubMed: 15738665]
15. Nair LS, Bhattacharyya S, Laurencin CT, Kumar Ce. Nanotechnology and Tissue Engineering: The Scaffold Based Approach. *Tissue, Cell and Organ Engineering.* 2006:1–56.
16. Lee CH, Shin HJ, Cho IH, Kang YM, Kim IA, Park KD, et al. Nanofiber alignment and direction of mechanical strain affect the ECM production of human ACL fibroblast. *Biomaterials.* 2005 Apr; 26(11):1261–1270. [PubMed: 15475056]
17. Baker SC, Atkin N, Gunning PA, Granville N, Wilson K, Wilson D, et al. Characterisation of electrospun polystyrene scaffolds for three-dimensional in vitro biological studies. *Biomaterials.* 2006 Jun; 27(16):3136–3146. [PubMed: 16473404]
18. Zhong S, Teo WE, Zhu X, Beuerman RW, Ramakrishna S, Yung LY. An aligned nanofibrous collagen scaffold by electrospinning and its effects on in vitro fibroblast culture. *J Biomed Mater Res A.* 2006 Dec 1; 79(3):456–463. [PubMed: 16752400]
19. Halliday NL, Tomasek JJ. Mechanical properties of the extracellular matrix influence fibronectin fibril assembly in vitro. *Exp Cell Res.* 1995 Mar; 217(1):109–117. [PubMed: 7867709]
20. Pelham RJ Jr, Wang Y. Cell locomotion and focal adhesions are regulated by substrate flexibility. *Proc Natl Acad Sci U S A.* 1997 Dec 9; 94(25):13661–13665. [PubMed: 9391082]
21. Wang MJH, Kaplan D, Rutledge G. Mechanical Properties of Electrospun Silk Fibers. *Macromolecules.* 2004; 37:6856–6864.

22. Karageorgiou V, Meinel L, Hofmann S, Malhotra A, Volloch V, Kaplan D. Bone morphogenetic protein-2 decorated silk fibroin films induce osteogenic differentiation of human bone marrow stromal cells. *J Biomed Mater Res A*. 2004 Dec 1; 71(3):528–537. [PubMed: 15478212]
23. Karageorgiou V, Tomkins M, Fajardo R, Meinel L, Snyder B, Wade K, et al. Porous silk fibroin 3-D scaffolds for delivery of bone morphogenetic protein-2 in vitro and in vivo. *J Biomed Mater Res A*. 2006 Aug; 78(2):324–334. [PubMed: 16637042]
24. Giancotti FG, Ruoslahti E. Integrin signaling. *Science*. 1999 Aug 13; 285(5430):1028–1032. [PubMed: 10446041]
25. Min BM, Lee G, Kim SH, Nam YS, Lee TS, Park WH. Electrospinning of silk fibroin nanofibers and its effect on the adhesion and spreading of normal human keratinocytes and fibroblasts in vitro. *Biomaterials*. 2004 Mar-Apr; 25(7–8):1289–1297. [PubMed: 14643603]
26. Bondar B, Fuchs S, Motta A, Migliaresi C, Kirkpatrick CJ. Functionality of endothelial cells on silk fibroin nets: Comparative study of micro- and nanometric fibre size. *Biomaterials*. 2007 Oct 15.
27. Garcia AJ, Vega MD, Boettiger D. Modulation of cell proliferation and differentiation through substrate-dependent changes in fibronectin conformation. *Mol Biol Cell*. 1999 Mar; 10(3):785–798. [PubMed: 10069818]
28. Vogel V, Baneyx G. The tissue engineering puzzle: a molecular perspective. *Annu Rev Biomed Eng*. 2003; 5:441–463. [PubMed: 14527318]
29. Sofia S, McCarthy MB, Gronowicz G, Kaplan DL. Functionalized silk-based biomaterials for bone formation. *J Biomed Mater Res*. 2001 Jan; 54(1):139–148. [PubMed: 11077413]
30. Li C, Vepari C, Jin HJ, Kim HJ, Kaplan DL. Electrospun silk-BMP-2 scaffolds for bone tissue engineering. *Biomaterials*. 2006 Jun; 27(16):3115–3124. [PubMed: 16458961]
31. Hino T, Tanimoto M, Shimabayashi S. Change in secondary structure of silk fibroin during preparation of its microspheres by spray-drying and exposure to humid atmosphere. *J Colloid Interface Sci*. 2003 Oct 1; 266(1):68–73. [PubMed: 12957583]
32. Jin HJ, Chen J, Karageorgiou V, Altman GH, Kaplan DL. Human bone marrow stromal cell responses on electrospun silk fibroin mats. *Biomaterials*. 2004 Mar; 25(6):1039–1047. [PubMed: 14615169]
33. Ochsner M, Dusseiller MR, Grandin HM, Luna-Morris S, Textor M, Vogel V, et al. Micro-well arrays for 3D shape control and high resolution analysis of single cells. *Lab Chip*. 2007 Aug; 7(8):1074–1077. [PubMed: 17653351]
34. Sun Y, Nelson BJ. MEMS capacitive force sensors for cellular and flight biomechanics. *Biomed Mater*. 2007; (2):S16–22. [PubMed: 18458415]
35. Smith ML, Gourdon D, Little WC, Kubow KE, Eguiluz RA, Luna-Morris S, et al. Force-induced unfolding of fibronectin in the extracellular matrix of living cells. *PLoS Biol*. 2007 Oct 2.5(10):e268. [PubMed: 17914904]
36. Baneyx G, Baugh L, Vogel V. Coexisting conformations of fibronectin in cell culture imaged using fluorescence resonance energy transfer. *Proc Natl Acad Sci U S A*. 2001 Dec 4; 98(25):14464–14468. [PubMed: 11717404]
37. Baugh L, Vogel V. Structural changes of fibronectin adsorbed to model surfaces probed by fluorescence resonance energy transfer. *J Biomed Mater Res A*. 2004 Jun 1; 69(3):525–534. [PubMed: 15127399]
38. Farndale RW, Buttle DJ, Barrett AJ. Improved quantitation and discrimination of sulphated glycosaminoglycans by use of dimethylmethylene blue. *Biochim Biophys Acta*. 1986 Sep 4; 883(2):173–177. [PubMed: 3091074]
39. Klotzsch E, Smith ML, Kubow KE, Gourdon D, Muntwyler S, Beyerle F, et al. Fibronectin forms the most elastic biological fibers. 2008 In preparation.
40. Negrin RS, Atkinson K, Leemhuis T, Hanania E, Juttner C, Tierney K, et al. Transplantation of highly purified CD34+Thy-1+ hematopoietic stem cells in patients with metastatic breast cancer. *Biol Blood Marrow Transplant*. 2000; 6(3):262–271. [PubMed: 10871151]
41. DeLisser HM, Newman PJ, Albelda SM. Platelet endothelial cell adhesion molecule (CD31). *Curr Top Microbiol Immunol*. 1993; 184:37–45. [PubMed: 8313722]

42. Zong XH, Kim K, Fang DF, Ran SF, Hsiao BS, Chu B. Structure and process relationship of electrospun bioabsorbable nanofiber membranes. *Polymer*. 2002; 43(16):4403–4412.
43. Fong H, Chung I, DHR. Beaded nanofibers formed during electrospinning. *Polymer*. 1999; 40(16): 4585–4592.
44. Jin HJ, Fridrikh SV, Rutledge GC, Kaplan DL. Electrospinning *Bombyx mori* silk with poly(ethylene oxide). *Biomacromolecules*. 2002 Nov-Dec;3(6):1233–1239. [PubMed: 12425660]
45. Sukigara S, Gandhi M, Ayutsede J, Micklus M, Ko F. Regeneration of *Bombyx mori* silk by electrospinning—part 1: processing parameters and geometric properties. *Polymer*. 2003; 44(19): 5721–5727.
46. Pham QP, Sharma U, Mikos AG. Electrospinning of polymeric nanofibers for tissue engineering applications: a review. *Tissue Eng*. 2006 May; 12(5):1197–1211. [PubMed: 16771634]
47. Mit-Uppatham C, Nithtanakal M, Supaphol P. Ultrafine electrospun polyamide-6 fibers: effect of solution conditions on morphology and average fibers diameter. *Macromol Chem Phys*. 2004; 205(17):2327–2338.
48. Caspar CL, Stephens JS, Tassi NG, Chase DB, Rabolt JF. Controlling surface morphology of electrospun polystyrene fibers: effect of humidity and molecular weight in the electrospinning process. *Macromolecules*. 2004; 37(2):573–578.
49. Um IC, Fang D, Hsiao BS, Okamoto A, Chu B. Electro-spinning and electro-blowing of hyaluronic acid. *Biomacromolecules*. 2004 Jul-Aug;5(4):1428–1436. [PubMed: 15244461]
50. Li WJ, Mauck RL, Cooper JA, Yuan X, Tuan RS. Engineering controllable anisotropy in electrospun biodegradable nanofibrous scaffolds for musculoskeletal tissue engineering. *J Biomech*. 2006 Oct 20.
51. Courtney T, Sacks MS, Stankus J, Guan J, Wagner WR. Design and analysis of tissue engineering scaffolds that mimic soft tissue mechanical anisotropy. *Biomaterials*. 2006 Jul; 27(19):3631–3638. [PubMed: 16545867]
52. Xu CY, Inai R, Kotaki M, Ramakrishna S. Aligned biodegradable nanofibrous structure: a potential scaffold for blood vessel engineering. *Biomaterials*. 2004 Feb; 25(5):877–886. [PubMed: 14609676]
53. Baker BM, Mauck RL. The effect of nanofiber alignment on the maturation of engineered meniscus constructs. *Biomaterials*. 2007 Apr; 28(11):1967–1977. [PubMed: 17250888]
54. Min BM, Jeong L, Lee KY, Park WH. Regenerated silk fibroin nanofibers: water vapor-induced structural changes and their effects on the behavior of normal human cells. *Macromol Biosci*. 2006 Apr 12; 6(4):285–292. [PubMed: 16572474]
55. Jin HJ, Park J, Karageorgiou V, Kim UJ, Valluzzi R, Cebe P, et al. Water-Stable Silk Films with Reduced -Sheet Content. *Adv Funct Mater*. 2005; (15):1241–1247.
56. Soffer L, Wang X, Zhang X, Kluge J, Dorfmann L, Kaplan DL, et al. Silk-based electrospun tubular scaffolds for tissue-engineered vascular grafts. *J Biomater Sci Polym Ed*. 2008; 19(5):653–664. [PubMed: 18419943]
57. Shao Z, Vollrath F, Yang Y, HCT. Structure and behavior of regenerated spider silk. *Macromolecules*. 2003; (36):1157–1161.
58. Peyton SR, Raub CB, Keschrumrus VP, Putnam AJ. The use of poly(ethylene glycol) hydrogels to investigate the impact of ECM chemistry and mechanics on smooth muscle cells. *Biomaterials*. 2006 Oct; 27(28):4881–4893. [PubMed: 16762407]
59. Pierschbacher MD, Ruoslahti E. Cell attachment activity of fibronectin can be duplicated by small synthetic fragments of the molecule. *Nature*. 1984 May 3–9; 309(5963):30–33. [PubMed: 6325925]
60. Mita K, Ichimura S, James TC. Highly repetitive structure and its organization of the silk fibroin gene. *J Mol Evol*. 1994 Jun; 38(6):583–592. [PubMed: 7916056]
61. Vogel V. Mechanotransduction involving multimodular proteins: converting force into biochemical signals. *Annu Rev Biophys Biomol Struct*. 2006; 35:459–488. [PubMed: 16689645]
62. Keselowsky BG, Collard DM, Garcia AJ. Integrin binding specificity regulates biomaterial surface chemistry effects on cell differentiation. *Proc Natl Acad Sci U S A*. 2005 Apr 26; 102(17):5953–5957. [PubMed: 15827122]

63. McClary KB, Ugarova T, Grainger DW. Modulating fibroblast adhesion, spreading, and proliferation using self-assembled monolayer films of alkythiolates on gold. *J Biomed Mater Res.* 2000 Jun 5; 50(3):428–439. [PubMed: 10737886]
64. Keselowsky BG, Collard DM, Garcia AJ. Surface chemistry modulates fibronectin conformation and directs integrin binding and specificity to control cell adhesion. *J Biomed Mater Res A.* 2003 Aug 1; 66(2):247–259. [PubMed: 12888994]
65. Bobis S, Jarocho D, Majka M. Mesenchymal stem cells: characteristics and clinical applications. *Folia Histochem Cytobiol.* 2006; 44(4):215–230. [PubMed: 17219716]
66. Docheva D, Popov C, Mutschler W, Schieker M. Human mesenchymal stem cells in contact with their environment: surface characteristics and the integrin system. *J Cell Mol Med.* 2007 Jan-Feb; 11(1):21–38. [PubMed: 17367499]
67. Majumdar MK, Keane-Moore M, Buyaner D, Hardy WB, Moorman MA, McIntosh KR, et al. Characterization and functionality of cell surface molecules on human mesenchymal stem cells. *J Biomed Sci.* 2003 Mar-Apr; 10(2):228–241. [PubMed: 12595759]
68. Karakecili AG, Demirtas TT, Satriano C, Gumusderelioglu M, Marletta G. Evaluation of L929 fibroblast attachment and proliferation on Arg-Gly-Asp-Ser (RGDS)-immobilized chitosan in serum-containing/serum-free cultures. *J Biosci Bioeng.* 2007 Jul; 104(1):69–77. [PubMed: 17697986]
69. Zong X, Bien H, Chung CY, Yin L, Fang D, Hsiao BS, et al. Electrospun fine-textured scaffolds for heart tissue constructs. *Biomaterials.* 2005 Sep; 26(26):5330–5338. [PubMed: 15814131]
70. Yang F, Murugan R, Wang S, Ramakrishna S. Electrospinning of nano/micro scale poly(L-lactic acid) aligned fibers and their potential in neural tissue engineering. *Biomaterials.* 2005 May; 26(15):2603–2610. [PubMed: 15585263]
71. He W, Yong T, Ma ZW, Inai R, Teo WE, Ramakrishna S. Biodegradable polymer nanofiber mesh to maintain functions of endothelial cells. *Tissue Eng.* 2006 Sep; 12(9):2457–2466. [PubMed: 16995779]
72. Wang JH, Jia F, Gilbert TW, Woo SL. Cell orientation determines the alignment of cell-produced collagenous matrix. *J Biomech.* 2003 Jan; 36(1):97–102. [PubMed: 12485643]

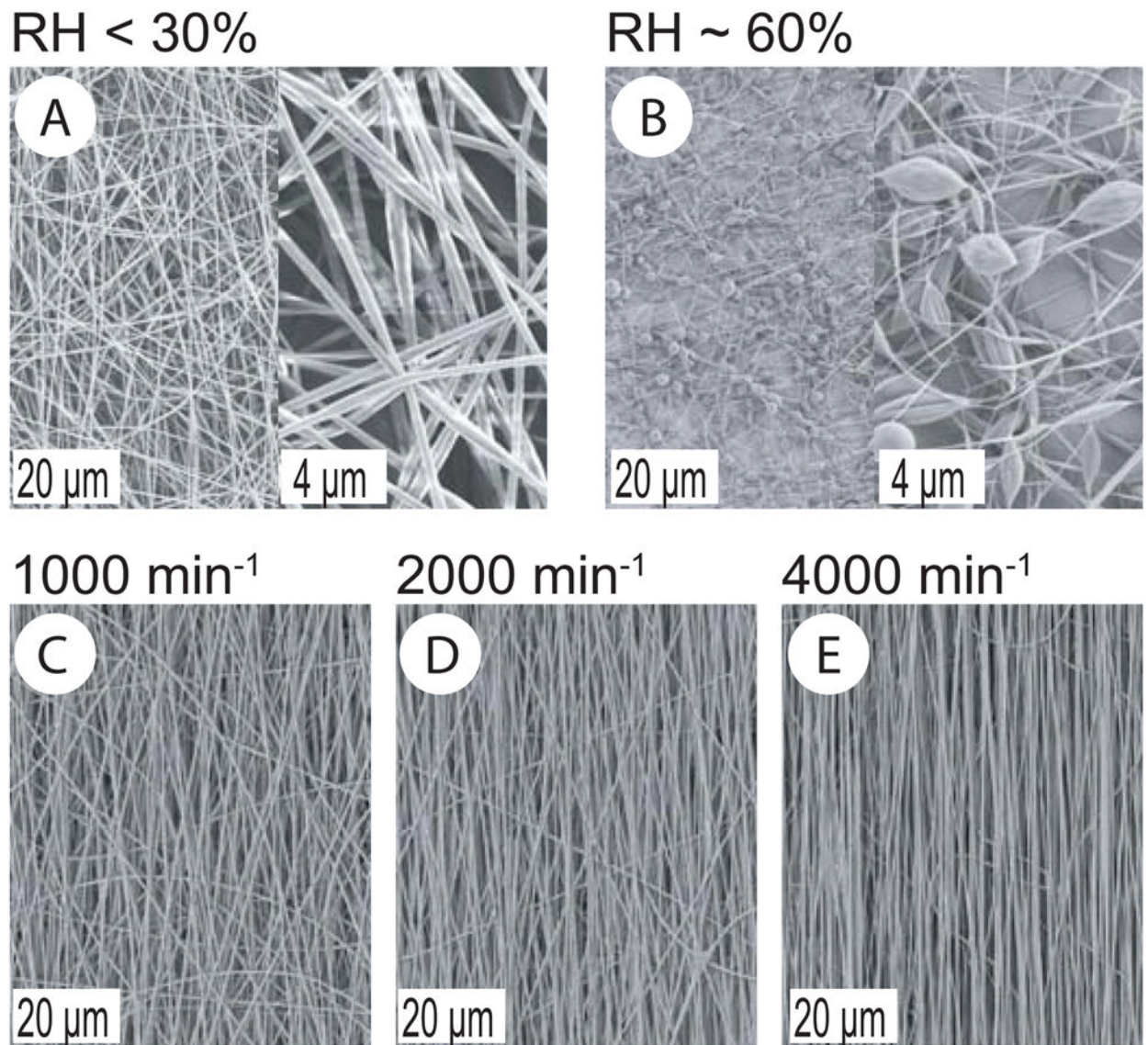


**Figure 1.** SEM micrographs of electrospun SF/PEO fibers at different humidities (A, B). SEM micrographs of SF/PEO fibers electrospun on a cylindrical target rotating with increasing speed (C–E).

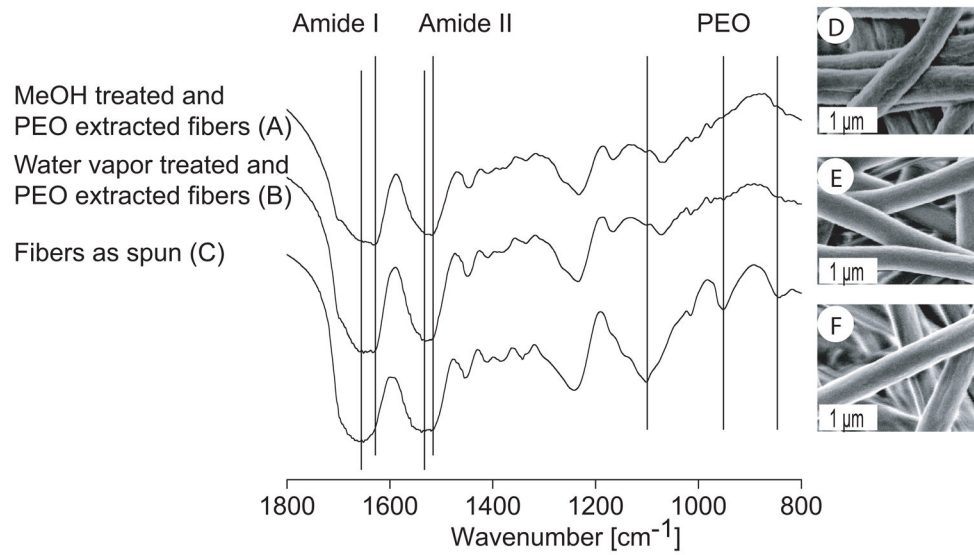


**Figure 2.** FT-IR spectra and SEM micrographs of electrospun fibers. MeOH (A, D) and water vapor treated fibers (B, E) after PEO extraction were compared to fibers as spun (C, F).

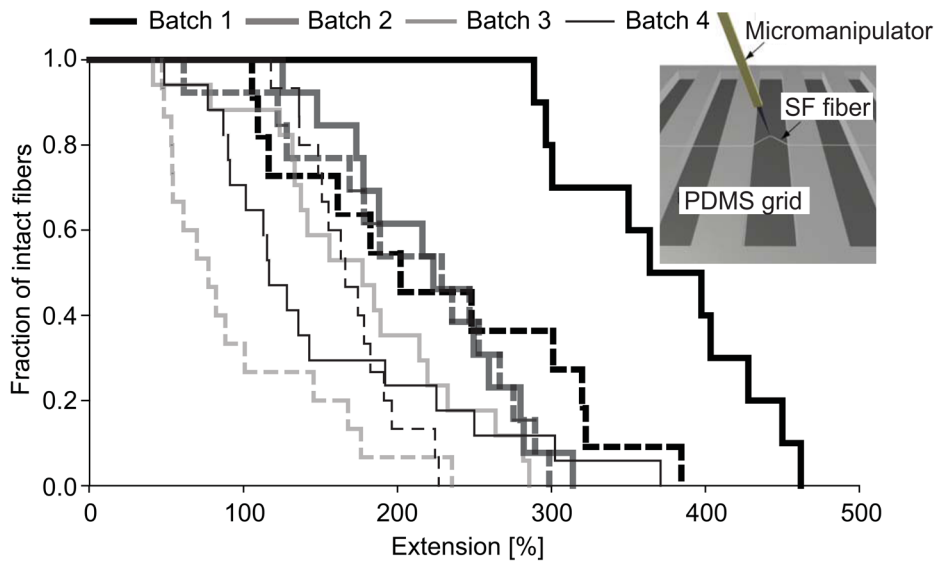


**Figure 3.** Extensibility of single electrospun SF fibers after MeOH (dashed line) or water vapor (solid line) treatment and PEO extraction. Data are shown for four different batches of fibers. A schematic image of the experimental setup is depicted in the insert.

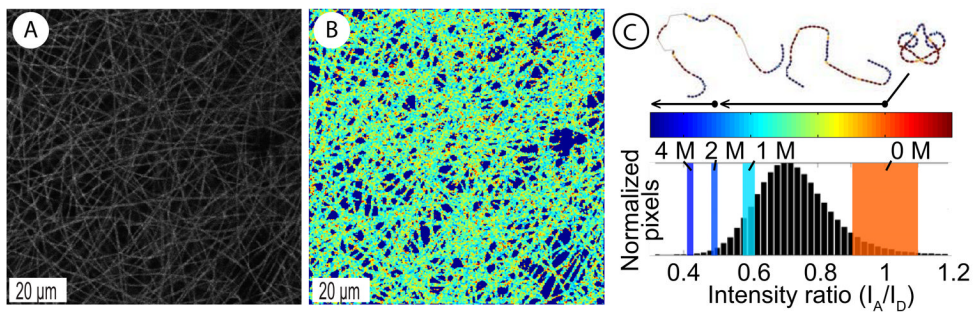


**Figure 4.** CLSM image of fluorescently labeled fibronectin adsorbed on electrospun random SF scaffold (A). IA/ID ratiometric image of acceptor to donor fluorophore intensity of adsorbed fibronectin-D/A (B). Histogram of all pixels in the field of view with overlaid solution denaturation values for fibronectin-D/A in 0–4 M GdnHCl. Hypothetical solution structures of fibronectin in denaturant are indicated by cartoons of compact, extended and partially unfolded fibronectin (C) and were presented before [35].

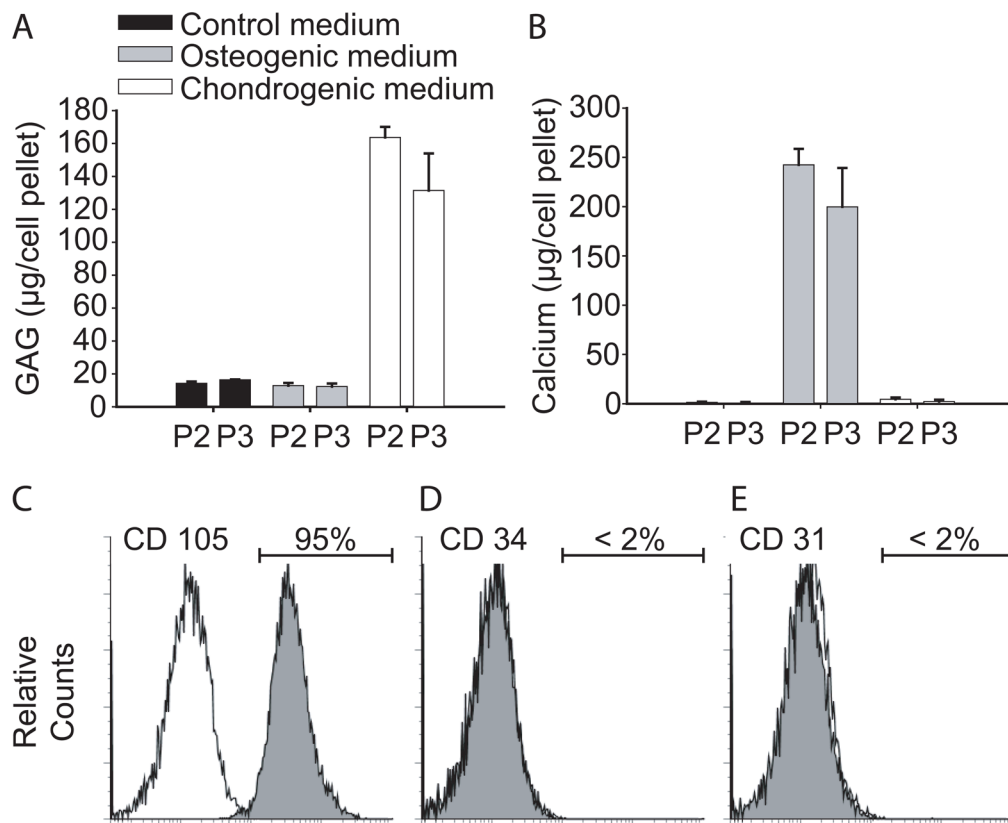


**Figure 5.** Characterization of hMSC. Deposition of GAG (A) and calcium (B) in passage 2 and 3 hMSC (P2, P3) in pellets cultured in either control, osteogenic or chondrogenic medium for 3 weeks. Flow cytometry with positive expression of the surface antigen CD 105 (C) and negative expression of CD34 (D) and CD 31 (E) on P2 hMSC.

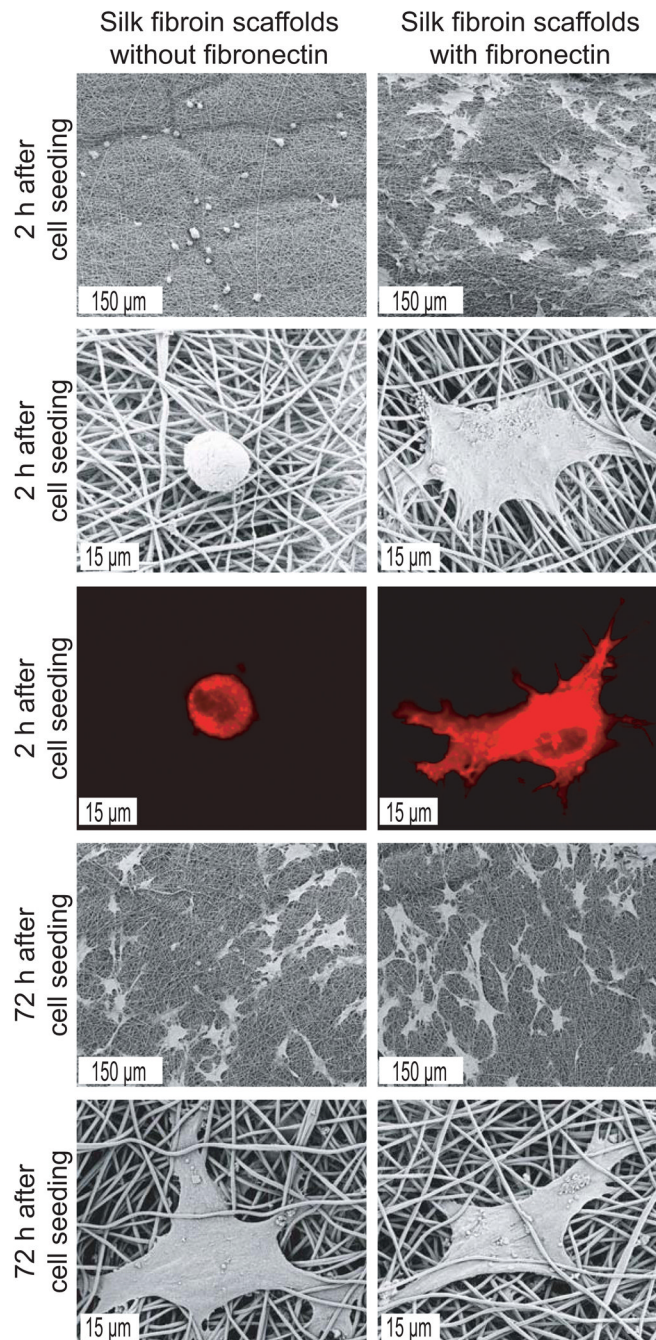


**Figure 6.** SEM and CLSM (membrane staining with DiI) micrographs of hMSC cultured for 2 and 72 h on electrospun random scaffolds with and without fibronectin coating.

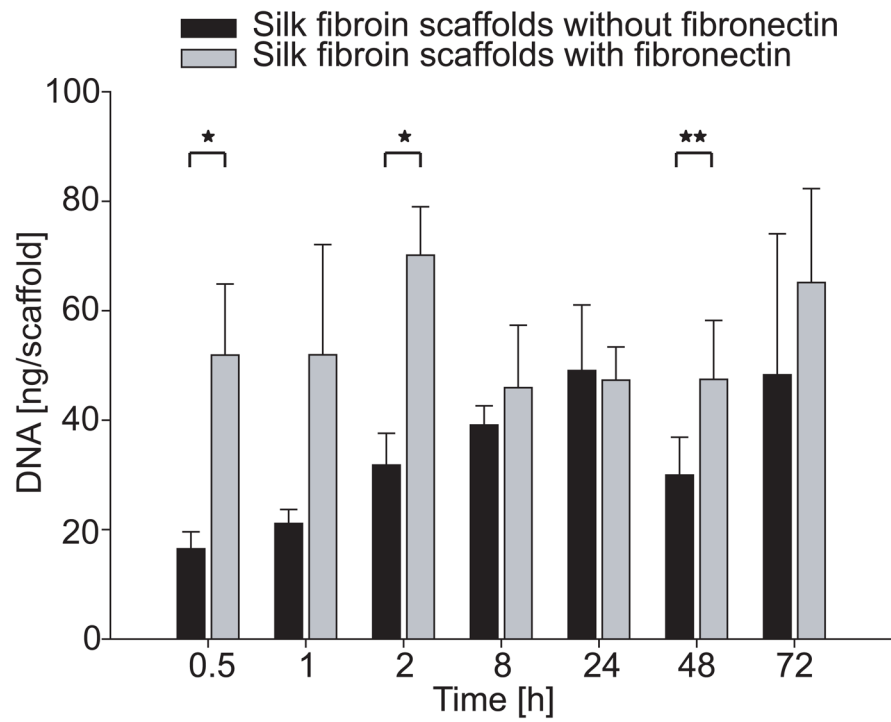


**Figure 7.** DNA content on electrospun random scaffolds after 0.5–72 h of hMSC culture. Asterisks indicate significant differences between scaffolds with and without fibronectin coating (\* $p < 0.01$ , \*\* $p < 0.05$ ).

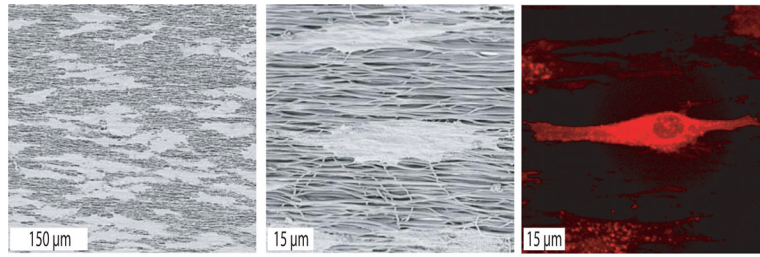


**Figure 8.** SEM and CLSM (membrane staining with DiI) micrographs of hMSC cultured for 2 h on fibronectin-coated aligned scaffolds.